Towards Palmprint Verification On Smartphones

Yingyi Zhang[1,2], **Lin Zhang**[1*], **Ruixin Zhang**[2], **Shaoxin Li**[2], **Jilin Li**[2], and **Feiyue Huang**[2]

[1]the School of Software Engineering, Tongji University
[2]Youtu Lab, Tencent

Abstract

With the rapid development of mobile devices, smartphones have gradually become an indispensable part of people's lives. Meanwhile, biometric authentication has been corroborated to be an effective method for establishing a person's identity with high confidence. Hence, recently, biometric technologies for smartphones have also become increasingly sophisticated and popular. But it is noteworthy that the application potential of palmprints for smartphones is seriously underestimated. Studies in the past two decades have shown that palmprints have outstanding merits in uniqueness and permanence, and have high user acceptance. However, currently, studies specializing in palmprint verification for smartphones are still quite sporadic, especially when compared to face- or fingerprint-oriented ones. In this paper, aiming to fill the aforementioned research gap, we conducted a thorough study of palmprint verification on smartphones and our contributions are twofold. First, to facilitate the study of palmprint verification on smartphones, we established an annotated palmprint dataset named MPD, which was collected by multi-brand smartphones in two separate sessions with various backgrounds and illumination conditions. As the largest dataset in this field, MPD contains 16,000 palm images collected from 200 subjects. Second, we built a DCNN-based palmprint verification system named DeepMPV+ for smartphones. In DeepMPV+, two key steps, ROI extraction and ROI matching, are both formulated as learning problems and then solved naturally by modern DCNN models. The efficiency and efficacy of DeepMPV+ have been corroborated by extensive experiments. To make our results fully reproducible, the labeled dataset and the relevant source codes have been made publicly available at https://cslinzhang.github.io/MobilePalmPrint/.

1 Introduction

Smartphones have become a necessity in people's lives and an important tool to perform daily work. With the increasing concern about networking and mobility security, the demand for reliable user authentication technology is also growing dramatically [1]. Propelled by the demand of various mobile applications, such as online payment and electronic banking, automatic identification of highly trusted people has become an intense study[2]. In fact, high-precision identity authentication for smartphones has long been one of the main focuses in the research field, such as fingerprint-based unlocking [3] and face-based e-payment [4].

However, ignored by many, palmprint is also a great choice for personal identity authentication. Palmprint [5, 6, 7] refers to the skin pattern on the inner surface of the palm, which mainly includes two characteristics: palm frictional ridges (ridges and valleys like fingerprints) and palm flexion creases (discontinuities in epidermal ridges). Palmprint, as an important member of the biometrics family, has many desired characteristics, such as strong uniqueness, durability and user-friendliness [8]. The ability of palmprints to discriminate different identities has been confirmed by numerous previous studies [9, 10]. In fact, palmprint authentication is a non-invasive way of authentication, which is more acceptable to users than facial authentication. Comparing fingerprint recognition with palmprint recognition, the former usually requires highly sensitive sensors, while the latter can be conducted by using the built-in camera of smartphones. In addition, some people do not have clear fingerprints, while palmprints have more abundant feature information and can be utilized in low-resolution conditions.

Although palmprint has many valuable merits as a biometric identifier, studies on palmprint recognition for smartphones are still quite rare, and consequently, the application potential of palmprints for smartphones is far from being fully explored. We attempt to fill this research gap by conducting a thorough study of palmprint verification on smartphones in this paper. A highly efficient and effective palmprint verification system specially designed for smartphone platforms is developed. In addition, a large-scale palmprint dataset collected by multi-brand smartphones is established and released to facilitate the further study of this area.

The remainder of this paper is organized as follows: Section 2 introduces related works and our contributions. Section 3 presents our DCNN-based palmprint verification system DeepMPV+ (short for "Lighter Deep-learning-based Mobile Palmprint Verification"). Section 4 states the details of MPD (short for "Mobile Palmprint Database"), which is our newly established benchmark dataset for the study of palmprint verification on smartphones. Experimental results are reported in Section 5. Finally, Section 6 concludes the paper.

2 Related Works and Our Contributions

In this section, we will first review some representative studies most relevant to our work, including approaches for palmprint ROI extraction, approaches for palmprint verification, and publicly available benchmark datasets. Then, we will present our motivations and contributions.

2.1 Approaches for Palmprint ROI Extraction

Most pipelines for palmprint recognition need to segment hands from the background before ROI extraction. Because of the unpredictable background and illumination of a mobile image, it is a challenging task to segment the hand from the rest of

*corresponding author: cslinzhang@tongji.edu.cn

the image. A common way is to define the hand region as skin pixels in the color space and to treat the rest as background pixels [11, 12, 13, 14], or use methods like the Otsu threshold to binarize the image [15, 16, 17]. Then, hands would be aligned for the next step. For this purpose, Franzgrote *et al.* in [11] resorted to hand orientation normalization, while Zhao *et al.* in [13] proposed a projection transformation model for estimating the matched SIFT feature points. In [18], Li *et al.* extracted principal lines from palms and used them to align hands. On the basis of hand segmentation and alignment, some schemes used valley detection [19], Harris corner detection [14] or radial distance functions [20] to locate key points and established the local coordinate system for palmprint ROI extraction, while others determined key points based on hand contours [21].

There are also some ROI extraction pipelines without relying on hand segmentation as a pre-processing step. In [22], Han *et al.* used a predefined preview frame on screen to align the position between hand and camera. When the palm was aligned, they cropped a sub-image of fixed size at a fixed position as ROI. Similar to Han *et al.*'s work [22], there are also methods such as hand-shaped guide window [23], double assistance points [24] and so on [25, 26, 27] to guide the user's hand gestures. Differently, Aykut *et al.* in [28] used an advanced hand model learned by AAM to obtain key points at the palm contour. Later in [8], Zhang *et al.* used a binary palm mask to locate the finger-gap-points to construct a local coordinate system. However, Zhang *et al.*'s method [8] can only be applied to images with uniform backgrounds.

2.2 Approaches for Palmprint Verification

In the field of palmprint verification, great efforts have been devoted to extracting features from palmprint ROIs. Existing schemes roughly fall into five branches.

The first branch of palmprint feature extraction schemes are coding-based methods. In a typical coding-based scheme, each field of the code map is assigned a bit-wised code, based on quantization of the image's response to a set of filters. Conventional coding-based schemes include PalmCode [5], CompCode [29], RLOC [30], OLOF [31], Accelerated CompCode [11], DRCC [33], and CR-CompCode [8]. Recently, some more advanced coding schemes that attempted to obtain more direction information such as DDBC [34] and ALDC [35], have been proposed.

The second branch is the line-based branch. These approaches typically extract palm lines using newly developed or off-the-shelf line detection operators. Palm lines are then matched directly [36, 37] or represented in other forms [38, 39] for matching.

The third branch is the subspace-based branch. These methods usually attempt to find a set of basis images from a training set and represent any probe image as a linear combination of them. Typical subspace-based methods for palmprint applications include PCA [40], CCA [41], LDA and ICA. On the basis of these methods, more advanced methods have been put forward, LPDP [42], Evo-KPCA [43] and so on. However, subspace-based methods are very sensitive to palmprint rotation, scaling and translation, and are not suitable for complex application scenarios such as mobile palmprint matching.

The fourth branch is the local-texture-descriptor-based branch. The first kind of local texture descriptors are designed for general applications but are adapted to the field of palmprint verification, such as LBP, HOG [44], SIFT [45] and LDP. In addition, local texture descriptors specially designed for palmprints have been proposed, and the typical ones include LBP+SIFT [7] and IHOL [46].

The fifth branch is the learning-based branch, which has attracted much attention in recent years. Most approaches in this branch simply make use of off-the-shelf CNN structures as palmprint feature encoders [47, 48, 49, 50, 51, 52, 53, 54]. Only a few of them aimed to design new CNN architectures to embed the special traits of palmprint images [55, 56, 57, 58].

2.3 Contactless Palmprint Datasets Publicly Available

To facilitate the design of palmprint matching algorithms, some researchers have collected benchmark contactless palmprint datasets and made them publicly available.

In [59], Hao *et al.* collected a normal palm image dataset and a multispectral palm image dataset (CASIA dataset and CASIA-multispectral[60], respectively). The former contains 5,502 palm images from 312 subjects in a single session while the latter contains 7,200 palm images captured from 100 different people in 2 separate sessions. For CASIA-multispectral, during each session, there are 3 samples and each sample includes 6 palm images captured under 6 different spectrum respectively. Furthermore, 4,800 images of CASIA-multispectral are palm-print images (taken under visible spectrums) and the other 2,400 ones are palm vein images (taken under IR spectrums). Meanwhile, Kumar [61] collected a contactless palmprint dataset (referred to as IIT-D [62]), in which images were captured from 235 subjects in a single session using a self-developed device. Later, Kanhangad *et al.* in [63] collected contactless 3D and 2D hand images to build the PolyU palmprint dataset II [64]. Kanhangad *et al.*'s dataset contains right-hand images from 114 subjects in 5 different poses. In [32], Ferrer *et al.* released a contactless palmprint dataset called GPDS100 [65]. GPDS100 comprises 2,000 samples that were acquired from 100 palms over two sessions. For each palm, GPDS100 kept 10 images. The dataset collected by Aykut *et al.* in [28] is referred to as KTU dataset [66], which comprises 1,752 images collected from 145 different palms in a single session. Concurrently, Hassanat *et al.* in [67] collected the MOHI dataset and WEHI dataset [68] using mobile phone cameras and webcams, respectively. More recently, Joshi *et al.* collected 1,344 high-resolution palm-print images from 168 subjects to compose the COEP palmprint database [69]. Zhang *et al.* [8] collected 12,000 palm images from 600 palms in two different sessions using their established contactless palmprint collection device, which is referred to as Tongji contactless palmprint dataset [70].

2.4 Our Motivations and Contributions

Through the study of relevant literature, we find that there is still much room for improvement in the field of palmprint verification for smartphones in at least two aspects.

First, large-scale datasets are quite rare in this field. To design palmprint verification systems for smartphones and also to objectively compare their performance, a public large-scale

benchmark dataset with various backgrounds and illumination conditions, collected by smartphones and carefully labeled, is indispensable. Unfortunately, thus far, the research community lacks such a dataset.

Second, effectively and accurately matching palmprints on smartphones remains a challenge. Due to the hardware limitation of smartphones and the speed requirements of mobile scenes, palmprint recognition on smartphones needs to meet both the requirements of light weight and fast speed. The performance of palmprint verification systems on smartphones still have much room for improvement, mainly regarding two tasks: palmprint ROI extraction and ROI matching.

1. Because of the complicated backgrounds and illumination conditions of palmprint images collected in uncontrolled environments, it is a challenging task to delineate palmprint ROIs accurately. In order to get rid of the influence of complex backgrounds in palmprint images, existing palmprint verification systems on smartphone usually need to segment hand at first, or request the user to place the hand in the designated position in front of the camera. The former is time-consuming and error-prone, while the latter is not user-friendly. Moreover, existing palmprint ROI extraction schemes hardly have the properties of scale and rotation invariance. In short, when the position of the hand is not ideal or the background is too complex, the performance of these methods is often unsatisfactory due to their inherent limitations.

2. In the phase of palmprint ROI matching, it is hard to discriminate whether two palmprint ROIs belong to the same hand due to the position deviation between the two ROIs or the difference of palmprint postures.

In this work, we attempt to fill the aforementioned research gaps to some extent. Our contributions are briefly summarized as follows:

1. To facilitate the study of palmprint verification on smartphones, we have established a large-scale palmprint dataset named MPD and have made it online available. MPD comprises 16,000 palm images collected from multi-brand smartphones and all the images are manually labeled with care. To our knowledge, it is currently the largest publicly available contactless palmprint dataset collected by smartphones in the unconstrained environment. Such a dataset will benefit the studies of palmprint recognition algorithms on smartphones. Please refer to Sect. 4 for more details about MPD.

2. We proposed a data-driven learning-based system named DeepMPV+ to verify palmprints on smartphones. Specifically, DeepMPV+ consists of two main modules, the ROI extraction module and the ROI matching module. Unlike the strategies reported in the literature, we creatively model the ROI extraction problem as an object detection problem, which can be naturally and effectively solved by modern CNNs. For these reasons, the proposed ROI extractor has the merits of being fast, accurate, and highly robust to complex backgrounds. In the stage of ROI matching, due to

the ability of ArcFace [71] to make different kinds of feature vectors more evenly and more independently located in the super feature space, and considering the hardware limitations and speed requirements of smartphones, a palmprint verifier based on MobileFaceNet [72] and ArcFace is used to match the extracted palmprint ROI. DeepMPV+ can work well on smartphones, and can match palmprint images with slight position offset and gesture deflection. The efficiency and performance of DeepMPV+ have been thoroughly evaluated in experiments.

3. Using the developed algorithms, we have implemented a practical palmprint verification system for the iPhone 8 Plus platform. As far as we know, it is the first reported smartphone-oriented palmprint verification system. To make our results fully reproducible, our collected dataset MPD and all the relevant code have been publicly released at https://cslinzhang.github.io/MobilePalmPrint/. Our research will prompt people to realize that palmprint is also a viable option for identity authentication on smartphones besides fingerprint and face.

A preliminary version of this manuscript has been accepted by ICME 2019 [73]. The following improvements are made in this version: 1) the whole pipeline is simplified from DeepMPV to DeepMPV+ with higher efficiency and performance, using 2 DCNN models instead of 3; 2) a thorough performance evaluation of modern DCNN models in the context of palmprint verification on smartphones is conducted, and higher-performance lightweight models are selected based on the experimental results; 3) the performance of palmprint recognition models and metrics used to measure the quality of palmprint recognition is thoroughly investigated and analyzed; and 4) additional relevant approaches are evaluated in experiments.

3 DeepMPV+: A Learning-Based Pipeline for Palmprint Verification

In this section, the proposed smartphone-oriented palmprint verification system DeepMPV+ is presented in detail. DeepMPV+ consists of two key components (as shown in Fig. 1), including palmprint ROI extraction and ROI verification. The details will be introduced in the following subsections.

3.1 Palmprint Image Annotation

When DCNNs are applied in the field of palmprint, a large-scale and carefully labeled palmprint image dataset is indispensable. First, the ground-truth of the object detection needs to be determined. For a palm image, the finger-gap-points (points at the junction of adjacent fingers, denoted as P_i and marked by the red points in Fig. 2(a)) between fingers are the most obvious visual feature areas. However, a local coordinate system cannot be established only by these disorderly finger-gap-points. Therefore, finger-gap-points cannot be directly used as regression objects for object detection.

To determine a local coordinate system, at least three points that are not on the same line need to be found. The first two points A and B of these three points are determined from the
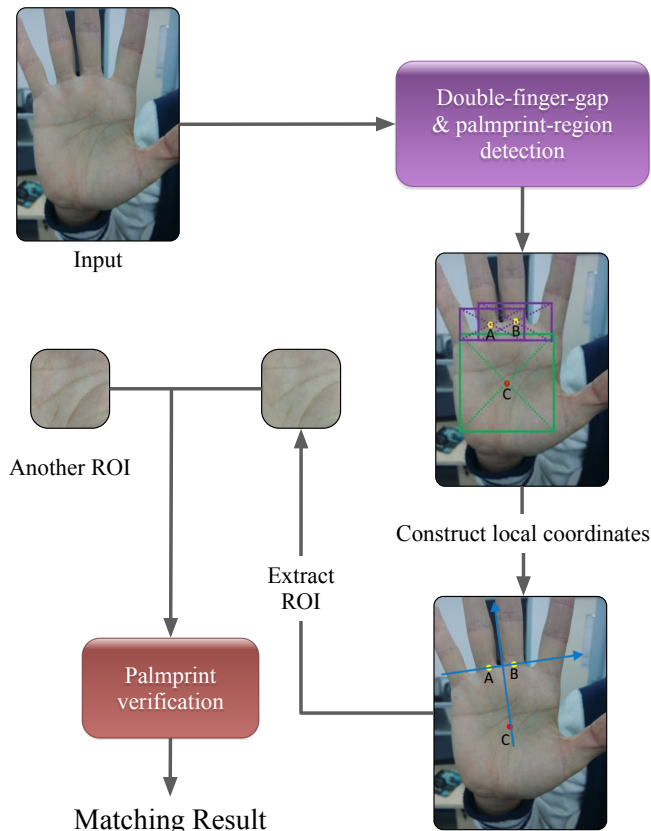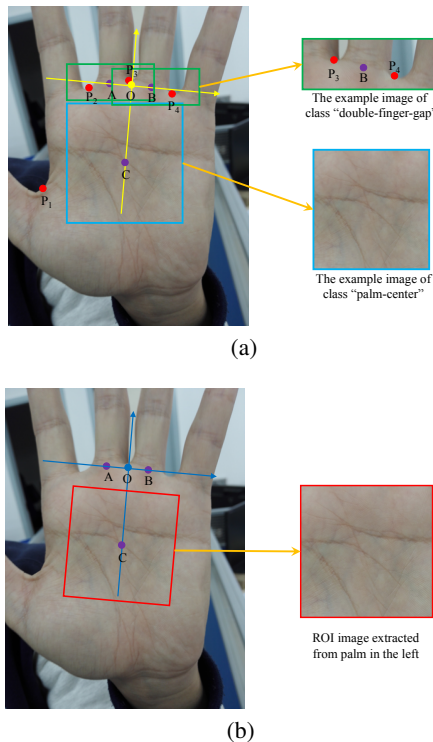
Figure 1: The system flowchart of *DeepMPV*.

Figure 2: Illustration of palm image annotation. (a) In the data annotation stage, we mark finger-gap-points (red points); the green rectangles indicate the double-finger-gaps while the blue rectangle represents the palm-center. (b) We use the well-trained detector D to obtain the position of point (A, B, C) and construct a local coordinate system (marked with blue arrows) to extract the *ROI* (marked as a red square).

aforementioned finger-gap-points. Point A is the midpoint of P_2P_3 while point B is the midpoint of P_3P_4. For these finger-gap-points, we name the point between the thumb and index finger as thumb-gap-point (the red point P_1 in Fig. 2(a)), while the other finger-gap-points are named as general-finger-gap-point (the red points $P_2 \sim P_4$ in Fig. 2(a)). To eliminate the interference of thumb-gap-points on detection, the double-finger-gap including one general-finger-gap-point pair ((P_2, P_3) or (P_3, P_4)) is regarded as the first class of object detection. The double-finger-gaps are marked with green rectangles in Fig. 2(a). Point A and point B are also the center points of two double-finger-gaps respectively. Based on them, the X-axis of the local coordinate system can be determined.

After determining point A and point B, point C is still needed to uniquely determine the local coordinate system. The midpoint O of AB is defined as the origin of the local coordinate system, and point C is defined as the point such that OC = $\frac{3}{2} \times \|AB\|$ that is located on both the Y-axis and the palm center area. The palm-center with point C as the center, containing the main palmprint area, is regarded as the second class of object detection, and is marked by the blue rectangle in Fig. 2(a).

In the stage of image annotation, all the finger-gap-points P_i are carefully labeled. We designate $\overrightarrow{AB}$ as the positive direction of the X-axis, establish the local coordinate system (marked with yellow arrows in Fig. 2(a)), and then calculate the position and area of the "double-finger-gap" and the "palm-center" based

on the aforementioned finger-gap-points. This position and area information will be used as the ground truth of the object detection model. Examples of the double-finger-gap and the palm-center are provided in Fig. 2(a).

3.2 Palmprint ROI Extraction

After data annotation, the next step is to train the object detection model. Having investigated the literature, we find that Tiny-YOLOV3 [74] is a state-of-the-art general-purpose object detector based on DCNN for mobile devices. Compared with MobileNetV1+SSD [75, 76], PeleeNet [77] and other lightweight networks, Tiny-YOLOV3 has higher speed and accuracy in real-time object detection on mobile devices. Hence, our detector D is based on Tiny-YOLOV3.

Given a palm image, the double-finger-gap is detected to obtain the coordinates of point pair (A, B), and the palm-center is detected to obtain the coordinates of point C. As shown in Fig. 2(b), the line through AB is defined as the line where the X-axis is located, while the direction perpendicular to AB and opposite to point C is defined as the positive direction of the Y-axis. The direction of the 90-degrees clockwise rotation of the Y-axis is the positive direction of the X-axis. With the midpoint O of AB as the origin, the local coordinate system for a given image is successfully established, which is marked with blue arrows in Fig. 2(b).

After the establishment of the local coordinate system, *ROI* is defined as a square area parallel to both the X-axis and the Y-axis. Suppose the coordinate of point O is (x_0, y_0), the center point of the *ROI* is set as $(x_0, y_0 + \frac{3}{2} \times \|AB\|)$, and its side length is set as s_R. The side length s_R is determined as $s_R = \frac{5}{2} \times \|AB\|$. Finally, we can extract the palmprint ROI from the palm image by extracting the image region covered by the *ROI* (marked as red square in Fig. 2(b)). The pipeline of palmprint ROI extraction is summarized in Algorithm 1.

Algorithm 1 Overall Pipeline of Palmprint ROI Extraction

Require: A palm image **I** and our detector **D**.
Ensure: Palmprint ROI image *ROI*.
 1: Feed **I** to **D** to obtain double-finger-gap center point set P_i^D and the palm-center center point C, where the size of set P_i^D is *L*;
 2: **if** $L > 2$ **then**
 3:     Traverse the set P_i^D, selecting point pairs;
 4:     Calculate the distance between two points;
 5:     Choose the two farthest points as (A,B);
 6: **else if** $L < 2$ **then**
 7:     **return** an indication of incomplete detection
 8: **end if**
 9: Set the line through AB as the X-axis;
10: Set the direction perpendicular to AB and opposite to point C as the positive direction of the Y-axis;
11: Set the midpoint of AB as the origin (x_0, y_0);
12: Take $\|AB\|$ as the unit length of axis;
13: Construct the local coordinate system;
14: Set the center coordinate of the *ROI* to $(x_0, y_0 + \frac{3}{2} \times \|AB\|)$;
15: Set the side length of *ROI* to $\frac{5}{2} \times \|AB\|$;
16: **return** segmented *ROI*

The details of **D**'s training set are shown in Sect. 4. In Sect. 5, we will quantitatively evaluate the performance of the detector **D**.

3.3 Palmprint Verification

For palmprint verification, the input is a pair of palmprint ROIs. In traditional methods, palmprint features are usually extracted to calculate matching scores. Therefore, the method used to extract palmprint features matters greatly. To extract the features of ROIs better, we used a DCNN-based method to fulfill the task. By studying the literature, we found that ArcFace[71] is very suitable for palmprint verification.

ArcFace uses an Additive Angular Margin Loss to obtain highly discriminative features from faces. It can make the feature vectors of different classes more uniform and independent in the super-feature space and help the model converge better. Moreover, considering the hardware limitations of the smartphone platform, after a detailed experiment and comparison based on the experimental results, we chose to use MobileFaceNet [72] as the backbone to extract palmprint features for matching. MobileFaceNet is a lightweight network designed for face verification and is an improved version of MobileNetV2 [79]. On the basis of MobileNetV2, in addition to the Additive Angular Margin Loss, it also used a Global Depthwise Convolution (GDConv) instead of Average Pooling layer, so that the network could treat

---

Algorithm 2 Overall Pipeline of Palmprint ROI Verification

Require: A pair of palmprint ROI images ROI_1 and ROI_2, our verifier **V**, and our threshold *T*.
Ensure: Matching result *R*.
 1: Resize ROI_1 and ROI_2 to the size 224×224;
 2: Feed ROI_1 and ROI_2 to **V** to obtain palmprint features F_1 and F_2, respectively;
 3: Use l_2-norm to normalize features F_1 and F_2 to obtain features $Fnorm_1$ and $Fnorm_2$, respectively
 4: Calculate matching score *S* by $S = Fnorm_1 \cdot Fnorm_2$;
 5: **if** $S >= T$ **then**
 6:     Set matching result *R* as "Matching Success";
 7: **else if** $S < T$ **then**
 8:     Set matching result *R* as "Matching Fail";
 9: **end if**
10: **return** matching result *R*.

---

the center point and the corner point differently when updating the weight. This model is very suitable for palmprint verification on smartphones, which is also an important reason for us to choose it. Therefore, our verifier **V** is based on MobileFaceNet and ArcFace.

Specifically, take a 224×224 palm ROI as the input. The 512×1 vector output by **V** is taken as the feature of this palm ROI. The final matching score can be obtained by performing a dot multiplication operation on the two palmprint ROI features. The threshold value to determine whether the match is successful is set to *T*, and the value of *T* is determined according to the experiments in Sect. 5.4. We took scores higher than *T* as matching success, otherwise, the palmprints matching fails. Details of the palmprint verification pipeline are shown in Algorithm 2.

More details of verifier **V**'s training set will be explained in Sect. 4. In Sect. 5, its performance will be quantitatively evaluated.

4 MPD: A Benchmark Dataset for Mobile Palmprint Verification

As stated in Sect. 2, in view of the fact that a database specially dedicated to mobile palmprint verification is still lacked in the community, and to provide a reasonable performance evaluation benchmark for palmprint verification on mobile platforms, we are motivated to establish such a dataset in this work. In this section, the establishment of our mobile palmprint database MPD is described. In total, MPD has 16,000 palmprint images from 200 subjects, and for each image there is an associated annotation with the position of finger-gap-points. The construction of MPD comprises two main steps: palm image collection and training and test set preparation. Details are given in the following subsections.

4.1 Palm Image Collection

To provide a reasonable performance evaluation benchmark for palmprint verification on mobile platforms, a large number of palm images were collected to compose our dataset MPD. MPD contains palm images with a variety of backgrounds and lighting environments. For the purpose of eliminating the influence of the camera parameters of different brands of mobile devices, two
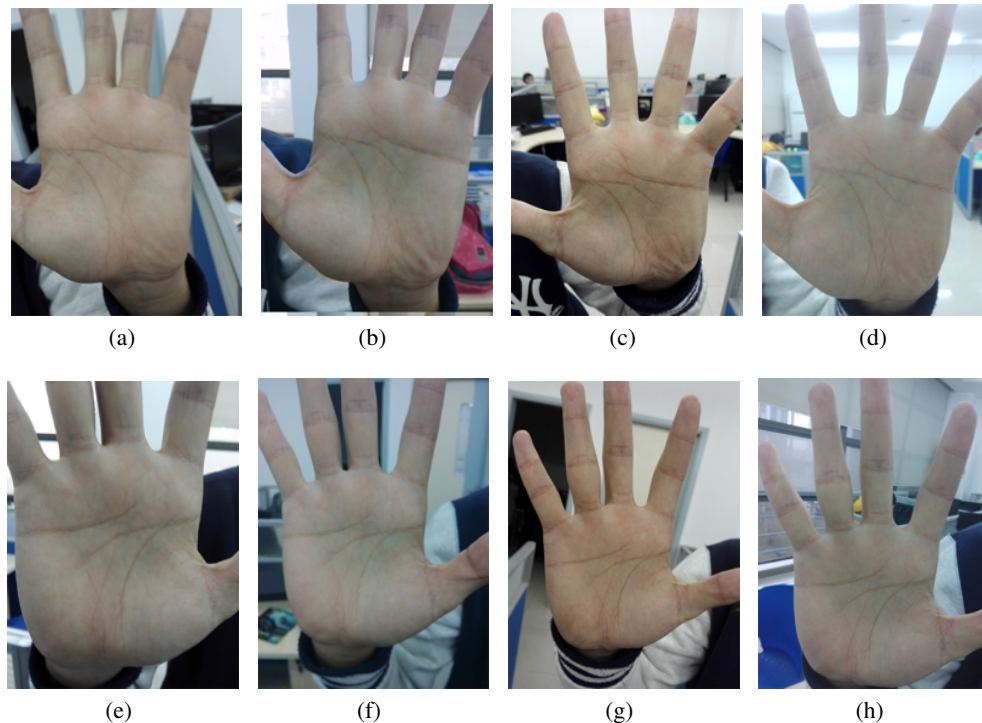
Figure 3: (a)~(h) are 8 images from the same person in our palmprint dataset MPD. (a)~(d) are left hand and (e)~(h) are the right hand. (a), (c), (e) and (g) were captured by Huawei, and (b), (d), (f) and (h) were captured by Xiaomi. (a), (b), (e) and (f) were collected in the first session, and (c), (d), (g) and (h) were collected in the second session.

kinds of smartphones were used to collect palm photos: Huawei and Xiaomi. To avoid the influence of the season or time on photographs, after the first round of collection, we took a group of photos with the same two mobile phones of the same group of people according to the same standard half a year later. MPD comprises 16,000 palmprint images from 200 volunteers. Those volunteers were staffs or students of Tongji University, with a balanced gender ratio. Among them, 195 subjects were $20 \sim 30$ years old and the others were $30 \sim 50$ years old. We obtained 10 photos of each subject's hand with each smartphone in each time period, which means there are 40 images of each hand and we have 400 different hands in our dataset. Furthermore, we labeled all 16,000 palm images in our dataset.

The palmprint images are named according to the following rules: 1) The first three digits, taking "001" as an example, indicate that this palm image was taken from the volunteer numbered 1; 2) the fifth digit, "1" for example, means that this palm image was taken in the first period; 3) for the seventh digit, "h" means that this palm image was taken by Huawei and "m" means this photo was taken by Xiaomi; 4) for the ninth digit, "l" indicates that this palm image was taken from the left hand of the volunteer and "r" indicates that this image was taken from the right hand; 5) the last two digits show the number of the palm image taken by the same volunteer with the same hand at the same time using the same smartphone. For instance, a palm image named "006_2_h_r_08.jpg" is a picture taken from the right hand of our sixth volunteer (No. 6) using Huawei mobile phone in the second period. Examples of palm images are shown in Fig. 3.
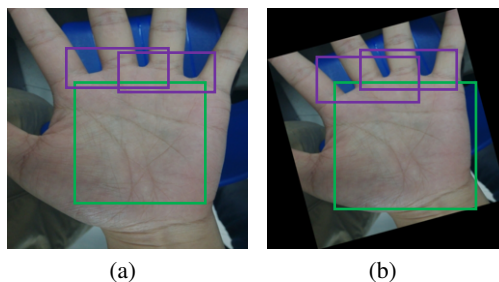

Figure 4: In the phase of preparing training samples, to make the detector D rotation invariant, each original labeled image was rotated to generate a set of its rotated versions. (a) is the original labeled image, and (b) is its rotated version generated from (a). The purple rectangles indicate the "double-finger-gap", and the green rectangles indicate the "palm-center".

4.2 Training and Test Set Preparation

In this section, the preprocessing and partitioning of each dataset will be introduced in detail. In dataset partitioning, palmprint detection and palmprint matching are regarded as open-set problems, and training set, verification set, and test set are guaranteed to have no overlap.

4.2.1 Generation and Preprocessing of D's Sets

In the training stage for our detector D, a training set was generated from the original dataset with annotations. The original dataset has annotations including the coordinates of finger-gap-

points (general-finger-gap-point and thumb-gap-point). Subsequently, the general-finger-gap-points are used to calculate the positions and areas of the "double-finger-gap" and "palm-center". As we can see in Fig. 4, the purple rectangles indicate the area of the "double-finger-gap", and the green square indicates the area of the "palm-center". For each palm image in our dataset, there are two marks of the class "double-finger-gap" and one mark of the class "palm-center" in general.

After generating the labels of our detector D's training set, to make it scale invariant, the training set was augmented by rotating each original labeled image to generate a number of its rotated versions as shown in Fig. 4. In detail, for a given original labeled image I, J rotated versions $\{I_j\}_{j=0}^{J-1}$ were obtained from it with a rotation angle $\theta_J = \frac{360}{J}$. To make the operation of rotation easier, the original labeled images were resized to a fixed size $s_f \times s_f$. Fig. 4(a) is an original labeled image, and Fig. 4(b) is its rotated version generated by Fig. 4(a) with a rotation of 15 degrees.

The augmented dataset was separated according to the following ratio: training set:validation set:test set = 8:1:1. The final training and test sets of detector D were named MPD_D (short for "The Dataset for Detector Generated from Mobile Palmprint Dataset").

4.2.2 Generation and Preprocessing of *V*'s sets

In the training stage for V, based on labeled data, the ROI dataset was generated with 16,000 images from 400 hands of 200 persons. It was named MPD_{ROI} (short for "The ROI Dataset Generated from Mobile Palmprint Dataset").

Since palmprint images acquired by smartphones often have different contrast, sharpness, and alignment quality, to improve the generalization ability of our verifier V, the following operations are performed for data augmentation. Two different models V_{IR} and V_{MBFN} have been applied with different data augmentation. And the details of these models are described in Sect. 5.2.

1. For V_{IR} in CASIA, (a) Resize to 246×246 and then random center crop, (b) ColorJintter: brightness and contrast are both 0.25, saturation is 0.2 and hue is 0.15 and (c) Horizontal Flip. For V_{MBFN} in CASIA, (a) Resize to 246×246 and then random center crop, (b) RandomResizedCrop: scale and ratio are both [0.9, 1.1], (c) ColorJintter: brightness and saturation are both 0.25, contrast and hue are both 0.15 and (d) Horizontal Flip.

2. For V_{IR} in IITD, (a) RandomResizedCrop: scale and ratio are both [0.75, 1.25], (b) ColorJintter: all the parameters are 0.15 and (c) Horizontal Flip. For V_{MBFN} in IITD, (a) RandomResizedCrop: scale and ratio are both [0.9, 1.1], (b) ColorJintter: all the parameters are 0.1, (c) RandomAffine: degress is [−5, 5], translate is [−0.05, 0.05], scale is [0.9, 1, 1] and shear is 0.1 and (d) Horizontal Flip.

3. For V_{IR} in PolyU, (a) RandomResizedCrop: scale and ratio are both [0.9, 1.1], (b) ColorJintter: brightness is 0.3, contrast is 0.25, saturation and hue are both 0.15 and (c) Horizontal Flip. For V_{MBFN} in PolyU, (a) RandomResizedCrop: scale and ratio are both [0.9, 1.1], (b)

ColorJintter: brightness is 0.25, the rest of parameters are all 0.15 and (c) Horizontal Flip.

4. For V_{IR} in TCD, (a) RandomResizedCrop: scale and ratio are both [0.8, 1.2], (b) ColorJintter: brightness and hue are both 0.1, the rest of parameters are 0.15, (c) Horizontal Flip and (d) Gaussian Noise: mean is 7, var is 0.1. For V_{MBFN} in TCD, (a) RandomResizedCrop: scale and ratio are both [0.9, 1.1], (b) ColorJintter: all the parameters are 0.1, (c) Horizontal Flip and (d) Gaussian Noise: mean is 7, var is 0.1.

5. For V_{IR} in MPD, (a) RandomResizedCrop: scale and ratio are both [0.75, 1.25], (b) ColorJintter: brightness is 0.25, the rest of parameters are all 0.15 and (c) Horizontal Flip. For V_{MBFN} in MPD, (a) RandomResizedCrop: scale and ratio are both [0.75, 1.25], (b) ColorJintter: brightness is 0.25, the rest of parameters are all 0.1 and (c) Horizontal Flip.

Ultimately, palmprint ROI images generated from 160 subjects were selected as the training set, and ROI images generated from the remaining 40 subjects formed the test set.

5 Experimental Results

5.1 Implementation Details of Detector D_{XS} in DeepMPV+

Five state-of-the-art or representative DCNN architectures, including PeleeNet+SSD [77, 76], ShuffleNet+SSD [78], MobileNetV1+SSD [75], MobileNetV2+SSD [79] and Tiny-YOLOV3[74], were investigated in the phase of detecting double-finger-gap and palm-center, and the corresponding concrete models for detector D_X are referred to as D_{PN}, D_{SN}, D_{MN1}, D_{MN2} and D_{YOLO}, respectively.

Table 1: Settings for the key hyper-parameters used when training D_{XS}

D_{XS}	Learning Rate	Optimizer	Batch Size	Weight Decay
D_{PN}	0.005	SGD	32	0.0005
D_{SN}	0.005	RMSProp	8	0.00005
D_{MN1}	0.005	RMSProp	16	0.00005
D_{MN2}	0.0005	RMSProp	8	0.0001
D_{YOLO}	0.001	-	16	0.0005

D_{XS} were trained on MPD_D. For training D_{XS}, we used the fine-tuning strategy, i.e., D_{XS} were fine-tuned from the deep models pre-trained on MS-COCO or VOC0712 for the task of object detection. Except for YOLO, Caffe was used as our deep learning platform when training models. Settings for key hyper-parameters used when training D_{XS}, including the learning rate, the optimizer, the batch size and the weight decay, are summarized in Table 1. In Table 1, "RMSProp" and "SGD" are two different optimization methods implemented in Caffe.

5.2 Implementation Details of Verifier V_{XS} in DeepMPV+

Taking ArcFace [71] as the training framework, two representative DCNN architectures, IR_50 [80] and MobileFaceNet [72],
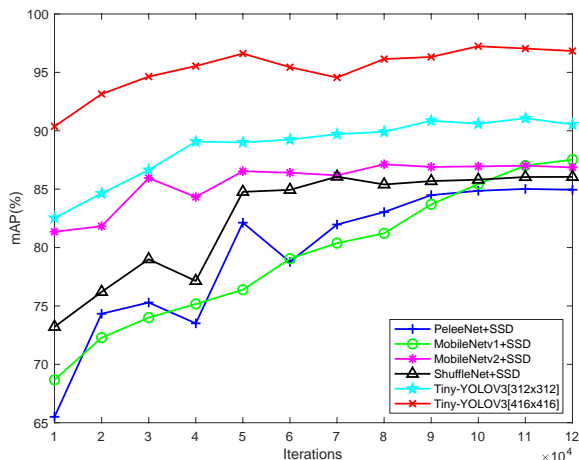
Figure 5: The mAP change curve during the training of D_Xs.

(a)

(b)

Figure 6: Keypoint detection results by different models. (a) shows the results of "double-finger-gap" while (b) shows the results of "palm-center".

were selected as backbones, and the corresponding V_X concrete models were called V_{IR} and V_{MBFN}, respectively.

Table 2: Settings for the key hyper-parameters used when training V_Xs

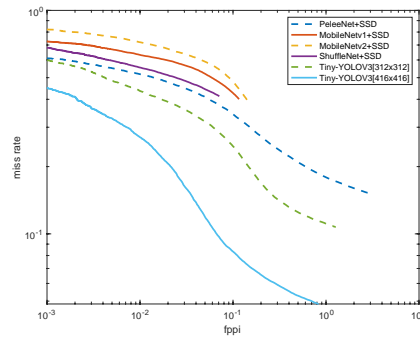| V_Xs	Learning Rate	Weight Decay	Epoch	Input Dimension
V_{IR}	0.005	0.0005	26	224×224
V_{MBFN}	0.005	0.0005	26	224×224

V_Xs were trained on multiple datasets including MPD$_{ROI}$. Pytorch was used as our deep learning platform when training models. Settings for key hyper-parameters used when training V_Xs, including the learning rate, weight decay, epochs and input dimension, are summarized in Table 2.
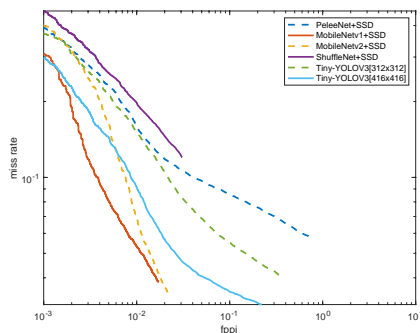
5.3 Evaluation of Detector D_Xs on MPD

Table 3: Sample table title

D_Xs	Input Dimension	Time Cost (ms)
D_{PN}	304×304	96.7
D_{SN}	300×300	85.8
D_{MN1}	300×300	99.6
D_{MN2}	300×300	105.5
D_{YOLO}	312×312	91.9
D_{YOLO}	**416×416**	**94.5**

In our palmprint verification system DeepMPV+, keypoint detection is a crucial step. As mentioned in Sect. 5.1, the performance of five DCNN-based methods was evaluated. The change curves of the mAP during the training stage of 5 models are illustrated in Fig. 5. As we can see, the mAP of D_{YOLO} reaches 96%, which is much higher than that of the other detectors. It is obvious that

the Tiny-YOLOV3-based model converged much faster than the other models according to Fig. 5.

All five models are implemented on iPhone 8 Plus, and the speed at which each image is processed is recorded. Table 3 lists the time costs of processing a single image. To eliminate the influence of the input image size, all the images were resized to approximately 300×300. Although D_{YOLO} takes 10 ms longer than D_{SN} to detect a single image, it is still reasonable to select the former because its mAP value is nearly 10% higher. Comparing two Tiny-YOLOV3-based models with different input dimensions, the model with the input dimension 416×416 is slower but much more accurate.

To better illustrate the performance of these 5 models, miss rate against false positives per image (FPPI) using log-log plots was plotted by varying the threshold on detection confidence. For a ground-truth keypoint g_i, if there is a detected keypoint d_i satisfying $\|g_i - d_i\| < \delta$, where δ is a predefined threshold, we deemed that g_i is correctly detected and d_i is a true positive. In this experiment, δ was set as 10. The figures were plotted for the "double-finger-gap" (Fig. 6(a)) and the "palm-center" (Fig. 6(b)). As recommended in [81], the log-average miss rate (LAMR) was used to summarize detector performance, computed by averaging miss rate at nine FPPI rates evenly spaced in log-space in the range 10^{-3} to 10^1. The LAMRs achieved by different models are also shown in Fig. 6. It is obvious that the Tiny-YOLOV3-based model with the input dimension 416×416 has the best

Table 4: 5-fold cross validation of detector D_{YOLO}

No.	AP of class 0 (%)	AP of class 1 (%)	mAP (%)
1	99.76	100.00	99.88
2	99.56	100.00	99.78
3	99.66	100.00	99.83
4	99.70	100.00	99.85
5	96.69	98.10	97.39
Average	99.05	99.62	99.35

performance on double-finger-gap detection according to Fig. 6(a). As seen from Fig. 6(b), MobileNetV1 and MobileNetV2 have better performance on palm-center detection. However, overall, the models based on Tiny-YOLOV3 have excellent performance on both classes. In short, Tiny-YOLOV3 outperforms other models in terms of the overall performance on MPD.

To better illustrate the performance of these 5 models, miss rate against false positives per image (FPPI) using log-log plots was plotted by varying the threshold on detection confidence. For a ground-truth keypoint g_i , if there is a detected keypoint d_i satisfying $\|g_i - d_i\| < \delta$, where δ is a predefined threshold, we deemed that g_i is correctly detected and d_i is a true positive. In this experiment, δ was set as 10. The figures were plotted for the "double-finger-gap" (Fig. 6(a)) and the "palm-center" (Fig. 6(b)). As recommended in [81], the log-average miss rate (LAMR) was used to summarize detector performance, computed by averaging miss rate at nine FPPI rates evenly spaced in log-space in the range 10^{-3} to 10^1. The LAMRs achieved by different models are also shown in Fig. 6. It is obvious that the Tiny-YOLOV3-based model with the input dimension 416×416 has the best performance on double-finger-gap detection according to Fig. 6(a). As seen from Fig. 6(b), MobileNetV1 and MobileNetV2 have better performance on palm-center detection. However, overall, the models based on Tiny-YOLOV3 have excellent performance on both classes. In short, Tiny-YOLOV3 outperforms other models in terms of the overall performance on MPD.

Table 5: 5-fold cross validation of detector D_{YOLO}

No.	AP of class 0 (%)	AP of class 1 (%)	mAP (%)
1	99.76	100.00	99.88
2	99.56	100.00	99.78
3	99.66	100.00	99.83
4	99.70	100.00	99.85
5	96.69	98.10	97.39
Average	99.05	99.62	99.35

To obtain a reliable and stable model, D_{YOLO} was cross-validated using 5-fold cross validation. Class 0 and class 1 in Table 5 indicate the class "double-finger-gap" and the class "palm-center", respectively. According to Table 5, D_{YOLO} performs well on our proposed MPD dataset.

In conclusion, we choose the Tiny-YOLOV3-based model with an input dimension of 416×416 as our final detector $\boldsymbol{D}$.

5.4 Evaluation of V_Xs on Multiple Datasets

To evaluate the performance of our proposed method, experiments were carried out on 5 contactless public palmprint image datasets including MPD. All these datasets are listed in detail in Table 6. For the convenience of recording, the PolyU II Palmprint Dataset will be recorded as PolyU and the Tongji Contactless Palmprint Dataset as TCD. For every dataset, the left and right palms of the same person are considered as belonging to different individuals. In addition, in the process of study, we considered using SiameseMobileNet [73] to match palmprints, which was eventually replaced by ArcFace+MobileFaceNet with better performance. More importantly, we compared the performance of the proposed method and the most recent methods in the literature on these datasets. Since most of the methods in the literature do not publish their source code, we re-implemented algorithms in some papers. To ensure the fairness of the comparison, we only compared methods with the same evaluation procedure. In addition, all experimental data of V_Xs are the average values after 5-fold cross validation to avoid bias.

5.4.1 Recognition Accuracy

At this stage, we chose to use the Top-1 Accuracy to evaluate the performance of all these methods. Specifically, for each palm (each ID), we randomly select an image as the registration image, take the rest of the images as input, and compare the selected image with the registration images one by one to find the ID of the input image. The Top-1 Accuracy is highly consistent with the real application scene, and it can represent the recognition performance of the methods well.

The recognition accuracy of V_Xs is compared with that of the most recent methods reported in the literature. To compare methods based on local texture descriptors, CompCode [29], OLOF [31], CR-CompCode [8], DDBC [34] and ALDC_M [35] are considered. To compare methods based on deep learning, we considered FERNet [54], PalmNet [58], VGG-16 [50], AlexNet-S [51], ResNet-50 [82], GoogLeNet [83] and PCANet [84]. Table 7 describes the Top-1 accuracy of V_Xs and the methods in the literature. As we can see, V_{IR}'s on the considered public palmprint datasets outperforms all these methods in the literature. In particular, V_{IR}'s Top-1 accuracy on the PolyU II reached 100%. Additionally, the Top-1 accuracy of V_{MBFN} in each dataset exceeded or approached that of the methods in the literature.

Table 6: Publicly Available Datasets Used

Name	Ref.	Year	Capture type	Features	N. img.	N. pal.	N. sess.
CASIA	[60]	2007	Contactless	Black background, uniform illumination conditions, slight hand pose variation and multi-spectrum.	5,502	624	1
IIT-D v1	[62]	2007	Contactless	Uniform background, uniform illumination conditions, slight hand pose variation.	2,601	460	1
PolyU II Palmprint Dataset	[64]	2011	Contactless	Uniform background, uniform illumination conditions, 5 hand postures, right hand, both 3D and 2D images.	1,140	114	1
Tongji Contactless Palmprint Dataset	[70]	2017	Contactless	Uniform background, uniform illumination conditions, constrained hand posture.	12,000	600	2
MPD	-	2020	Smartphones	Uncontrolled background, multiple illumination conditions, various hand postures.	16,000	400	2

Notes: N. img. = Number of images; N. pal. = Number of palms; N. sess. = Number of sessions.

Table 7: Top-1 Accuracy (%) of V_Xs and other methods in literature

Method	CASIA	IIT-D	PolyU II	TCD	MPD
PalmNet-GaborPCA*	97.17	97.31	99.95	99.89	91.88
FERNet	97.65	99.61	99.77	98.63	-
VGG-16	97.80	93.64	-	98.46	-
AlexNet-S	92.76	97.24	70.96	-	-
ResNet-50	95.21	95.57	54.92	-	-
GoogLeNet	93.84	96.22	68.59	-	-
PCANet	95.53	97.37	99.66	-	-
DDBC	96.41	96.44	-	98.73	-
ALDC_M	94.64	97.00	99.85	-	-
CompCode	79.27	77.79	99.21	-	-
OLOF	73.32	73.26	99.55	-	-
CR-CompCode	91.73	94.22	97.18	-	-
Siamese-MobileNet	53.47	59.30	86.76	92.98	78.53
V_{IR}	**98.91**	**99.85**	**100.00**	**99.90**	**99.18**
V_{MBFN}	**98.11**	99.19	**99.97**	99.81	**98.06**

*Re-implemented using official public code.

Table 8: EERs (%) of V_Xs and other methods in literature

Method	CASIA	IIT-D	PolyU II	TCD	MPD
PalmNet-GaborPCA*	3.21	3.83	0.39	0.40	6.22
FERNet	0.73	0.76	0.15	-	-
VGG-16	7.86	7.44	-	2.86	-
AlexNet-S	1.79	0.92	14.91	-	-
ResNet-50	4.27	3.68	13.45	-	-
GoogLeNet	1.65	1.97	11.19	-	-
PCANet	1.46	1.18	0.45	-	-
CompCode	1.08	1.39	0.68	-	-
OLOF	1.75	2.09	0.23	-	-
CR-CompCode	3.18	2.78	1.02	-	-
Siamese-MobileNet	9.72	5.24	2.18	1.38	3.03
V_{IR}	**0.59**	**0.47**	**0.08**	**0.21**	**0.81**
V_{MBFN}	0.85	**0.74**	0.19	**0.34**	**1.28**

*Re-implemented using official public code

5.4.2 Verification Accuracy

In this phase, we chose to use the Equal Error Rate (EER) to evaluate the performance of these methods because it is one of the most commonly used metrics for biometric verification. We compared V_Xs with learning-based methods such as FERNet [54] and PalmNet [58], VGG-16 [50], AlexNet-S [51], ResNet-50 [82], GoogLeNet [83] and PCANet [84], and local-texture-descriptor-based methods like CompCode [29], OLOF [31] and CR-CompCode [8]. Table 8 details the EERs of V_Xs and the methods in the literature. It can be seen from Table 8 that the performance of V_{IR} on these public palmprint datasets is better than that of all the methods in the literature, while the EER of V_{MBFN} on each dataset exceeded or approached the methods in the literature.

Table 9: The average feature extraction (per image) and comparison time (ms) of different methods

Method	Ref.	Feature Extraction	Comparison
PalmNet-GaborPCA	[58]	1600.0000	10.0000
DDBC	[34]	26.5000	2.0000
ALDC	[35]	78.5000	0.1000
V_{IR}	-	1230.6132	**0.0018**
V_{MBFN}	-	100.4943	**0.0018**

Table 10: TPRs (%) with FAR=10^{-1}, FAR=10^{-2}, FAR=10^{-3} and FAR=10^{-4} of V_Xs and other methods on MPD

Method	FAR=10^{-1}	FAR=10^{-2}	FAR=10^{-3}	FAR=10^{-4}
PalmNetGaborPCA	95.17	88.02	81.64	76.28
SiameseMobileNet	99.62	88.60	51.89	15.56
V_{IR}	**99.82**	**99.28**	**96.53**	**94.20**
V_{MBFN}	**99.66**	**98.49**	**94.97**	**89.53**

5.4.3 Time Cost

We measured the time consumed by each method to extract features from a single palmprint image and compare a pair of palmprint images, which are listed in Table 9. ArcFace calculates the similarity of a pair of palmprint features by a multiplicative way, which is very fast and takes approximately 1.77×10^{-6}s, almost negligible. The speed of each method in Table 9 in feature extraction can be roughly divided into two levels: 100ms level (DDBC, ALDC and V_{MBFN}) and 1000ms level (PalmNet and V_{IR}). Considering the memory limitation and speed requirement of smartphones, we chose the final verifier in 100ms level, and finally chose V_{MBFN} with the best performance in 100ms level as our final verifier V.

5.4.4 Determination of Threshold

Finally, we used True Positive Rate (TPR)-False Acceptance Rate (FAR) to determine the matching threshold of DeepMPV+. We tested TPR-FAR on MPD, which is the most complex dataset at present. Table 10 details the TPR-FAR for V_Xs and other methods. It can be seen from Table 10 that V_Xs are obviously superior to other methods. According to this table, for the sake of security, we chose the threshold corresponding to V_{MBFN} when FAR=10^{-4} as the final threshold T to build a smartphone palmprint verification application, $T = 0.5014$.

5.5 Application System Implementation

A practical palmprint verification system was implemented as an iOS application on iPhone 8 Plus. Illustrations of its interfaces are shown in Fig. 7. We will introduce our interfaces according to the user's steps.

When a user enters our application, the first page he or she will see is the home page, as shown in Fig. 7(a). The user then simply clicks the camera button in the center of the home page to scan his or her palmprint for authentication. However, if the user is using our application for the first time, it means he/she may not have registered his/her palmprint yet. We will remind the user to register his/her palmprint as shown in Fig. 7(b).

Before matching palmprints, the user's palmprint ROI images need to be stored in our local database. As we can see, Fig. 7(c)~7(e) are the registration pages of our system. When the user enters the registration page for the first time, he/she will see the page with blank hand buttons as shown in Fig. 7(c). To avoid the impact of poorly photographed palm images, 3 palmprint ROI images are stored for each palm. When the user stores one palmprint ROI image, one-third of the palm buttons turn black,

as shown in Fig. 7(d). Therefore, if the user has completed the registration of personal palmprint information, the hand button will turn to completely black, as illustrated in Fig. 7(e). If the user wants to reset his/her palm information, he/she only needs to click the hand button and re-store 3 palm images. The button will return to the blank state and change to the full black state during the user's reset operation.

When the user completes the registration of his/her palmprint information, he/she can use the camera to take palm images and match palmprints. If the user clicks the camera button, he/she will come to the scan pages like Fig. 7(f) and Fig. 7(g). In general, our system will detect 2 double-finger-gaps and 1 palm-center in one hand. Fig. 7(f) is a scan screenshot of the left hand while Fig. 7(g) is a scan screenshot of the right hand. The user clicks the white circle button to save the photo of his/her palm. Real-time detection boxes can help users find better positions and angles for photo capture.

Once the user clicks the white circle button, our system will capture palm images, detect feature regions to construct a local coordinate system and extract palmprint ROIs. The ROI image will be compared with pre-stored palmprint ROI images, and the highest score for palmprint verification will be selected. If the score is greater than T, the system will go back to the home page and give the feedback "Palmprint Verification Success" (as shown in Fig. 7(h)); otherwise, the system will give the feedback "Palmprint Verification Fail" (as shown in Fig. 7(i)).

In the phase of scanning palmprint, if the palmprint ROI cannot be extracted due to poor photography of the palmprint, our system will return to the home page and tell the user "Scan fail, please take photo again".

6 Conclusion and Future Work

In this paper, we made two major contributions to the field of vision-based palmprint verification. First, we collected and labeled a large-scale palmprint dataset including 16,000 palm images from 200 subjects using multi-brand smartphones, which is the largest one in this field. We have made it publicly available. Such a dataset will surely benefit the study of palmprint verification. Second, we proposed a DCNN-based solution for palmprint verification on mobile platforms. Its high efficiency and efficacy have been corroborated by experiments. Extensive experiments conducted on palmprint verification indicate that our proposed model DeepMPV+ can surpass all its competitors.

In the near future, we will try to refine our DCNN-based palmprint verification solution and to continuously enlarge MPD to include more palmprint samples. Furthermore, we will also try to improve our method by incorporating few-shot learning.

References

[1] A. K. Jain, P. Flynn, and A. A. Ross, *Handbook of Biometrics*. New York, USA: Springer Sci. & Bus. Med., 2007.

[2] T. J. Neal and D. L. Woodard, "Surveying biometric authentication for mobile device security," *J. Pattern Recognit. Research*, vol. 1, pp. 74–110, 2016.
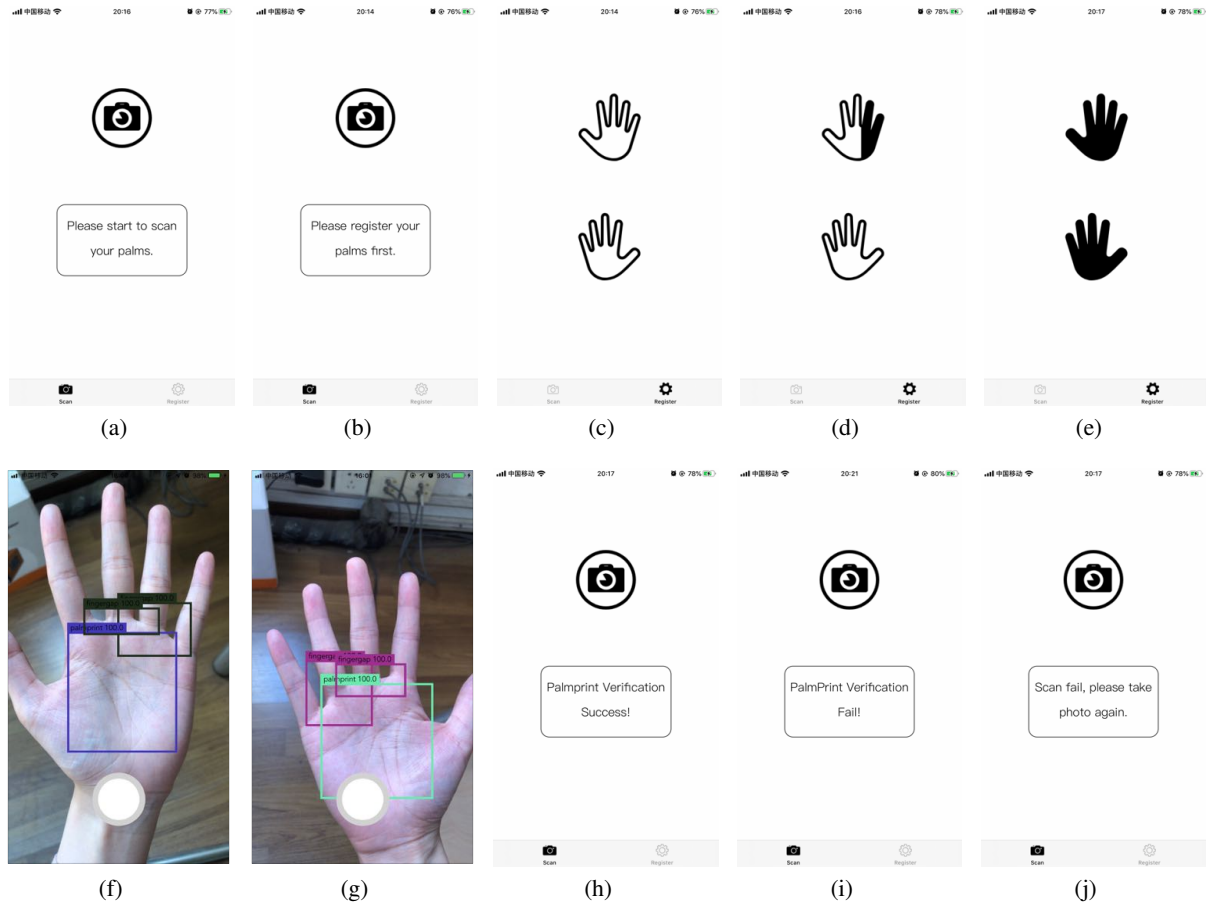
Figure 7: (a)~(j) are 10 screenshots of our palmprint verification application. (a) is the home and (b) is the hint page that suggests users to set up their palm images; (c), (d) and (e) are registration pages while (f) and (g) are the pages dynamically showing the process of ROI detection; (h), (i) and (j) are the pages showing the ultimate verification results.

[3] H. Co., "Huawei mate 20 pro," https://consumer.huawei.com/en/phones/mate20-pro/, in-screen Fingerprint.

[4] A. Co., "Face ID: Your face is your password." https://www.apple.com/iphone-xs/face-id/, apple Face ID.

[5] D. Zhang, W. Kong, J. You, and M. Wong, "Online palmprint identification," *IEEE Trans. Pattern Anal. Mach. Intell.*, vol. 25, no. 9, pp. 1041–1050, 2003.

[6] L. Zhang, Y. Shen, H. Li, and J. Lu, "3D palmprint identification using block-wise features and collaborative representation," *IEEE Trans. Pattern Anal. Mach. Intell.*, vol. 37, no. 8, pp. 1730–1736, 2015.

[7] H. Javidnia, A. Ungureanu, and P. Corcoran, "Palm-print recognition for authentication on smartphones," in *Proc. IEEE Int'l Symposium Technol. Society*. IEEE, 2015, pp. 1–5.

[8] L. Zhang, L. Li, A. Yang, Y. Shen, and M. Yang, "Towards contactless palmprint recognition: A novel device, a new benchmark, and a collaborative representation based identification approach," *Pattern Recognit.*, vol. 69, pp. 199–212, 2017.

[9] W. Meng, D. S. Wong, S. Furnell, and J. Zhou, "Surveying the development of biometric user authentication on mo-

bile phones," *IEEE Commun. Surv. Tutor.*, vol. 17, no. 3, pp. 1268–1293, 2014.

[10] D. Zhong, X. Du, and K. Zhong, "Decade progress of palmprint recognition: A brief survey," *Neurocomputing*, vol. 328, pp. 16–28, 2019.

[11] M. Franzgrote, C. Borg, B. J. T. Ries, S. Bussemaker, X. Jiang, M. Fieleser, and L. Zhang, "Palmprint verification on mobile phones using accelerated competitive code," in *Proc. Int'l Conf. Hand-Based Biometrics*. IEEE, 2011, pp. 1–6.

[12] M. Choraś and R. Kozik, "Contactless palmprint and knuckle biometrics for mobile devices," *Pattern Anal. Appl.*, vol. 15, no. 1, pp. 73–85, 2012.

[13] Q. Zhao, W. Bu, and X. Wu, "SIFT-based image alignment for contactless palmprint verification," in *Proc. Int'l Conf. Biometrics*. IEEE, 2013, pp. 1–6.

[14] A. Ungureanu and C. Costache, "Palm print as a smartphone biometric: Another option for digital privacy and security," *IEEE Consum. Electron. Magaz.*, vol. 5, no. 3, pp. 71–78, 2016.

[15] A. de Santos S., C. Sánchez-Ávila, A. M. Ormaza, and J. G. Casanova, "An approach to hand biometrics in mobile

devices," *Signal Image Video Process.*, vol. 5, no. 4, p. 469, 2011.

[16] N. F. Moco, I. S. Técnico, I. de Telecomunicações, and P. L. Correia, "Smartphone-based palmprint recognition system," in *Proc. Int'l Conf. Telecommunications*. IEEE, 2014, pp. 457–461.

[17] T. Chai, S. Wang, and D. Sun, "A palmprint ROI extraction method for mobile devices in complex environment," in *Proc. IEEE Int'l Conf. Signal Processing*. IEEE, 2016, pp. 1342–1346.

[18] W. Li, B. Zhang, L. Zhang, and J. Yan, "Principal line-based alignment refinement for palmprint recognition," *IEEE Trans. Syst. Man, and Cybern. Part C*, vol. 42, no. 6, pp. 1491–1499, 2012.

[19] A. Ungureanu, S. Thavalengal, T. Cognard, C. Costache, and P. Corcoran, "Unconstrained palmprint as a smartphone biometric," *IEEE Trans. Consum. Electron.*, vol. 63, no. 3, pp. 334–342, 2017.

[20] S. Aoyama, K. Ito, T. Aoki, and H. Ota, "A contactless palmprint recognition algorithm for mobile phones," in *Int'l Workshop Advance. Image Technol.*, 2013, pp. 409–413.

[21] L. Fang and Neera, "Mobile based palmprint recognition system," in *Proc. Int'l Conf. Control Automation Robotics*. IEEE, 2015, pp. 233–237.

[22] Y. Han, T. Tan, Z. Sun, and Y. Hao, "Embedded palmprint recognition system on mobile devices," in *Proc. Int'l Conf. Biometrics*. Springer, 2007, pp. 1184–1193.

[23] J. S. Kim, G. Li, B. Son, and J. Kim, "An empirical study of palmprint recognition for mobile phones," *IEEE Trans. Consum. Electron.*, vol. 61, no. 3, pp. 311–319, 2015.

[24] F. Gao, L. Leng, and J. Zeng, "Palmprint recognition system with double-assistant-point on iOS mobile devices," in *Pro. British Mach. Vis. Conf.*, 2018.

[25] G. Putra, I. Putra, and P. Buana, "Android based palmprint recognition system," *Telkomnika*, vol. 12, no. 1, p. 263, 2014.

[26] K. Tiwari, C. J. Hwang, and P. Gupta, "A palmprint based recognition system for smartphone," in *Future Technol. Conf.*. IEEE, 2016, pp. 577–586.

[27] L. Leng, F. Gao, Q. Chen, and C. Kim, "Palmprint recognition system on mobile devices with double-line-single-point assistance," *Pers. Ubiquitous Comput.*, vol. 22, no. 1, pp. 93–104, 2018.

[28] M. Aykut and M. Ekinci, "Developing a contactless palmprint authentication system by introducing a novel roi extraction method," *Image Vis. Comput.*, vol. 40, pp. 65–74, 2015.

[29] A. Kong and D. Zhang, "Competitive coding scheme for palmprint verification," in *Proc. Int'l Conf. Pattern Recognit.*, vol. 1. IEEE, 2004, pp. 520–523.

[30] W. Jia, D. Huang, and D. Zhang, "Palmprint verification based on robust line orientation code," *Pattern Recognit.*, vol. 41, no. 5, pp. 1504–1513, 2008.

[31] Z. Sun, T. Tan, Y. Wang, and S. Li, "Ordinal palmprint representation for personal identification," in *Proc. IEEE Conf. Comput. Vis. Pattern Recognit.*, vol. 1. IEEE, 2005, pp. 279–284.

[32] M. A. Ferrer, F. Vargas, and A. Morales, "Bispectral contactless hand based biometric system," in *CONATEL*. IEEE, 2011, pp. 1–6.

[33] Y. Xu, L. Fei, J. Wen, and D. Zhang, "Discriminative and robust competitive code for palmprint recognition," *IEEE Trans. Syst. Man Cybern. Syst.*, vol. 48, no. 2, pp. 232–241, 2016.

[34] L. Fei, B. Zhang, Y. Xu, Z. Guo, J. Wen, and W. Jia, "Learning discriminant direction binary palmprint descriptor," *IEEE Trans. Image Processing*, vol. 28, no. 8, pp. 3808–3820, 2019.

[35] L. Fei, B. Zhang, W. Zhang, and S. Teng, "Local apparent and latent direction extraction for palmprint recognition," *Inform. Sciences*, vol. 473, pp. 59–72, 2019.

[36] X. Wu, D. Zhang, and K. Wang, "Palm line extraction and matching for personal authentication," *IEEE Trans. Syst. Man Cybern. Part A-Syst. Hum.*, vol. 36, no. 5, pp. 978–987, 2006.

[37] D. Huang, J. Wei, and D. Zhang, "Palmprint verification based on principal lines," *Pattern Recognit.*, vol. 41, no. 4, pp. 1316–1328, 2008.

[38] L. Zhang and D. Zhang, "Characterization of palmprints by wavelet signatures via directional context modeling," *IEEE Trans. Syst. Man Cybern. Part B-Cybern.*, vol. 34, no. 3, pp. 1335–1347, 2004.

[39] Y. Xu, L. Fei, and D. Zhang, "Combining left and right palmprint images for more accurate personal identification," *IEEE Trans. Image Processing*, vol. 24, no. 2, pp. 549–559, 2014.

[40] K. Cheung, A. Kong, D. Zhang, M. Kamel, and J. You, "Does eigenpalm work? A system and evaluation perspective," in *Proc. Int'l Conf. Pattern Recognit.*, vol. 4. IEEE, 2006, pp. 445–448.

[41] Z. Wang, C. Liu, T. Shi, and Q. Ding, "Face-palm identification system on feature level fusion based on CCA," *J. Inform. Hiding and Multimedia Signal Processing*, vol. 4, no. 4, pp. 272–279, 2013.

[42] J. Gui, W. Jia, L. Zhu, S. Wang, and D. Huang, "Locality preserving discriminant projections for face and palmprint recognition," *Neurocomputing*, vol. 73, no. 13-15, pp. 2696–2707, 2010.

[43] S. Ibrahim, H. Jaafar, and D. A. Ramli, "Robust palm print verification system based on evolution of kernel principal component analysis," in *Proc. IEEE Int'l Conf. Control Syst. Comput. Engineering*. IEEE, 2014, pp. 202–207.

[44] W. Jia, R. Hu, Y. Lei, Y. Zhao, and J. Gui, "Histogram of oriented lines for palmprint recognition," *IEEE Trans. Syst. Man Cybern. Syst.*, vol. 44, no. 3, pp. 385–395, 2013.

[45] A. Genovese, V. Piuri, and F. Scotti, *Touchless Palmprint Recognition Systems*. Basel, Switzerland: Springer Int'l Publish., 2014, vol. 60.

[46] M. Arunkumar and S. Valarmathy, "Palm print identification using improved histogram of oriented lines," *Circuits Syst.*, vol. 7, no. 08, p. 1665, 2016.

[47] A. Jalali, R. Mallipeddi, and M. Lee, "Deformation invariant and contactless palmprint recognition using convolutional neural network," in *Proc. Int'l Conf. Human-Agent Interact.*. ACM, 2015, pp. 209–212.

[48] S. Minaee and Y. Wang, "Palmprint recognition using deep scattering convolutional network," *arXiv preprint arXiv:1603.09027*, 2016.

[49] A. Meraoumia, F. Kadri, H. Bendjenna, S. Chitroub, and A. Bouridane, "Improving biometric identification performance using PCANet deep learning and multispectral palmprint," in *Biometric Secur. Privacy*. Springer, 2017, pp. 51–69.

[50] A. S. Tarawneh, D. Chetverikov, and A. B. Hassanat, "Pilot comparative study of different deep features for palmprint identification in low-quality images," *arXiv:1804.04602*, 2018.

[51] R. Ramachandra, K. B. Raja, S. Venkatesh, S. Hegde, S. D. Dandappanavar, and C. Busch, "Verifying the newborns without infection risks using contactless palmprints," in *Proc. Int'l Conf. Biometrics*. IEEE, 2018, pp. 209–216.

[52] M. Izadpanahkakhk, S. M. Razavi, M. Taghipour-Gorjikolaie, S. H. Zahiri, and A. Uncini, "Joint feature fusion and optimization via deep discriminative model for mobile palmprint verification," *Jour. Electron. Imaging*, vol. 28, no. 4, p.043026, 2019.

[53] D. Zhong and J. Zhu, "Centralized large margin cosine loss for open-set deep palmprint recognition," *IEEE Trans. Circuits Syst. Video Technol.*, to appear.

[54] W. M. Matkowski, T. Chai, and A. W. K. Kong, "Palmprint recognition in uncontrolled and uncooperative environment," *IEEE Trans. Inform. Forensics and Secur.*, to appear.

[55] J. Svoboda, J. Masci, and M. M. Bronstein, "Palmprint recognition via discriminative index learning," in *Proc. Int'l Conf. Pattern Recognit.*. IEEE, 2016, pp. 4232–4237.

[56] J. Zhang, A. Yang, M. Zhang, and Q. Zhang, "Bidirectional aggregated features fusion from cnn for palmprint recognition," *Int'l J. Biometrics*, vol. 10, no. 4, pp. 334–351, 2018.

[57] K. Zhou, X. Zhou, L. Yu, L. Shen, and S. Yu, "Double biologically inspired transform network for robust palmprint recognition," *Neurocomputing*, vol. 337, pp. 24–45, 2019.

[58] A. Genovese, V. Piuri, K. N. Plataniotis, and F. Scotti, "Palmnet: Gabor-pca convolutional networks for touchless palmprint recognition," *IEEE Trans. Inform. Forensics and Secur.*, vol. 14, no. 12, pp. 3160–3174, 2019.

[59] Y. Hao, Z. Sun, T. Tan, and C. Ren, "Multispectral palm image fusion for accurate contact-free palmprint recognition," in *Proc. IEEE Int'l Conf. Image Processing*. IEEE, 2008, pp. 281–284.

[60] "CAISA Multi-Spectral Palmprint Database," http://biometrics.idealtest.org/dbDetailForUser.do?id=6, [Online].

[61] A. Kumar, "Incorporating cohort information for reliable palmprint authentication," in *Proc. Indian Conf. Comput. Vis. Graph. Image Processing*. IEEE, 2008, pp. 583–590.

[62] "IIT Delhi Touchless Palmprint Database," http://www4.comp.polyu.edu.hk/~csajaykr/IITD/Database_Palm.htm, [Online].

[63] V. Kanhangad, A. Kumar, and D. Zhang, "Contactless and pose invariant biometric identification using hand surface," *IEEE Trans. Image Processing*, vol. 20, no. 5, pp. 1415–1424, 2010.

[64] "The Hong Kong Polytechnic University Contact-free 3D/2D Hand Images Database (Version 2.0)," http://www4.comp.polyu.edu.hk/~csajaykr/Database/3Dhand/Hand3DPose.htm, [Online].

[65] "GPDS100 Contactless Hands 2Band Database," http://www.gpds.ulpgc.es/downloadnew/download.htm, [Online].

[66] "Ktu cvpr lab. contactless palmprint database," http://ceng2.ktu.edu.tr/~cvpr/contactlessPalmDB.htm, [Online].

[67] A. Hassanat, M. Al-Awadi, E. Btoush, A. Al-Btoush, E. Alhasanat, and G. Altarawneh, "New mobile phone and webcam hand images databases for personal authentication and identification," *Proced. Manufact.*, vol. 3, pp. 4060–4067, 2015.

[68] "Hand Images Databases," https://xwww.mutah.edu.jo/biometrix/hand-images-databases.html, [Online].

[69] Autonomous Institute of Government of Maharashtra, "COEP Palm Print Database," http://www.coep.org.in/resources/coeppalmprintdatabase, [Online].

[70] "Tongji Palmprint Dataset," http://sse.tongji.edu.cn/linzhang/contactlesspalm/index.htm, [Online].

[71] J. Deng, J. Guo, N. Xue, and S. Zafeiriou, "Arcface: Additive angular margin loss for deep face recognition," in *Proc. IEEE Conf. Comput. Vis. Pattern Recognit.*, 2019, pp. 4690–4699.

[72] S. Chen, Y. Liu, X. Gao, and Z. Han, "Mobilefacenets: Efficient cnns for accurate real-time face verification on mobile devices," in *Proc. Chinese Conf. Biometric Recognit.*. Springer, 2018, pp. 428–438.

[73] Y. Zhang, L. Zhang, X. Liu, S. Zhao, Y. Shen, and Y. Yang, "Pay by showing your palm: A study of palmprint verification on mobile platforms," in *Proc. IEEE Int'l Conf. Multimedia and Expo*. IEEE, 2019, pp. 862–867.

[74] J. Redmon and A. Farhadi, "Yolov3: An incremental improvement," *arXiv:1804.02767*, 2018.

[75] A. G. Howard, M. Zhu, B. Chen, D. Kalenichenko, W. Wang, T. Weyand, M. Andreetto, and H. Adam, "Mobilenets: Efficient convolutional neural networks for mobile vision applications," *arXiv:1704.04861*, 2017.

[76] W. Liu, D. Anguelov, D. Erhan, C. Szegedy, S. Reed, C. Fu, and A. C. Berg, "SSD: Single shot multibox detector," in *Proc. European Conf. Comput. Vis.*. Springer, 2016, pp. 21–37.

[77] R. J. Wang, X. Li, S. Ao, and C. X. Ling, "Pelee: A real-time object detection system on mobile devices," *arXiv:1804.06882*, 2018.

[78] X. Zhang, X. Zhou, M. Lin, and J. Sun, "ShuffleNet: An Extremely Efficient Convolutional Neural Network for Mobile Devices," in *arXiv preprint*, arXiv:1707.01083, 2017.

[79] M. Sandler, A. Howard, M. Zhu, A. Zhmoginov, and L. Chen, "Inverted residuals and linear bottlenecks: Mobile networks for classification, detection and segmentation," *arXiv:1801.04381*, 2018.

[80] C. Szegedy, S. Ioffe, V. Vanhoucke, and A. A. Alemi, "Inception-v4, inception-resnet and the impact of residual connections on learning," in *Proc. AAAI Conf. Artificial Intelligence*, 2017.

[81] P. Dollar, C. Wojek, B. Schiele, and P. Perona, "Pedestrian detection: An evaluation of the state of the art," *IEEE Trans. Pattern Anal. Mach. Intell.*, vol. 34, no. 4, pp. 743–761, 2011.

[82] K. He, X. Zhang, S. Ren, and J. Sun, "Deep residual learning for image recognition," in *Proc. IEEE Conf. Comput. Vis. Pattern Recognit.*, 2016, pp. 770–778.

[83] C. Szegedy, W. Liu, Y. Jia, P. Sermanet, S. Reed, D. Anguelov, D. Erhan, V. Vanhoucke, and A. Rabinovich, "Going deeper with convolutions," in *Proc. IEEE Conf. Comput. Vis. Pattern Recognit.*, 2015, pp. 1–9.

[84] T.-H. Chan, K. Jia, S. Gao, J. Lu, Z. Zeng, and Y. Ma, "PCANet: A simple deep learning baseline for image classification?" *IEEE Trans. Image Processing*, vol. 24, no. 12, pp. 5017–5032, 2015.